Solution Structure of Apo CopZ from *Bacillus subtilis*: Further Analysis of the Changes Associated with the Presence of Copper[†]

Lucia Banci, Ivano Bertini,* and Rebecca Del Conte

Department of Chemistry and Centro di Risonanze Magnetiche, University of Florence, Via Luigi Sacconi 6, 50019, Sesto Fiorentino, Italy

Received July 25, 2003

ABSTRACT: The solution structure of apo CopZ from *Bacillus subtilis* has been determined with the aim of investigating the changes in the hydrophobic interactions around the M-X-C-X-X-C copper(I) binding motif upon metal binding. The methionine of this motif (Met 11 in CopZ) points toward the solvent in apo CopZ, whereas its sulfur atom is close to the metal ion in the metal-loaded protein, though probably not at binding distance. This change is associated with the weakening of the interaction between Leu 37 and Cys 16, present in the apo form, and the formation of an interaction between Met 11 and Tyr 65. Loops 1, 3, and 5 are affected by metal binding. Comparison with the structure of other homologous proteins confirms that often metal binding affects a hydrophobic patch around the metal site, possibly for optimizing and tuning the hydrophobic interactions with the partners. It is also shown that copper(I) exchanges among apo CopZ molecules in slow exchange on the NMR time scale, whereas it is known that such exchange between partner molecules (i.e., metallochaperones and metal pumps) is fast.

Transition metal ion uptake, transport, and accumulation are tightly regulated by a complex machinery of proteins which bind the metal ions, transfer through membranes, and guide the metal ions through the cytoplasm to their final destinations. It is also becoming clear that these transport proteins employ atypical coordination properties (*1*−*4*).

The M-X-C-X-X-C motif is a highly conserved metal binding motif particularly found in proteins involved in metal homeostasis, where the two cysteine residues are the metal binding ligands (*5*). This motif is found in copper(I)-transporting proteins, but it is also present in proteins involved in binding and transport of other metal ions, such as Zn(II), Cd(II), and Hg(II) (*1*, *6*−*8*). The factors determining the metal specificity are, however, not yet fully elucidated even though the experimental structures (either in solution or in the crystal) are now becoming available, in some cases both with and without the metal ion. These structures share a completely conserved fold, constituted by the classical $\beta\alpha\beta\beta\alpha\beta$ ferredoxin fold, and a similar metal binding region (*4*, *9*). The Met side chain of this consensus motif, located in loop 1, often points toward an hydrophobic patch of the protein in most of the structures. This hydrophobic patch is determined by interactions between loop 1 and loops 3 and/or 5.

The structure of the copper-loaded *Bacillus subtilis*[1] CopZ (BsCopZ hereafter) (*10*), a soluble copper transport protein, shows that this Met residue is pointing toward the metal ion from the side of the solvent instead of pointing toward an internal hydrophobic patch (*10*). This structure as well as those of homologous proteins shows that several other groups screen the metal ion from solvent accessibility, although no potential donor atom has been proposed to be at binding distances (*1*, *4*, *11*). These residues are located where the process of metal transfer from a protein to another occurs, so that their presence might have some relevance.

In an attempt to gain further insight on the role of this residue and of the hydrophobic interactions as they depend on metal binding, we have characterized the apo form of BsCopZ and compared the conformational properties in a series of related proteins upon metal binding.

EXPERIMENTAL PROCEDURES

Sample Preparation. Apo BsCopZ was expressed, following a procedure already reported (*10*), in BL21(DE3)-pLysS cells containing the pET21-*bscopz* plasmid. ^{15}N-Labeled protein was obtained by growing the *Escherichia coli* OD2-N cells in labeled Silantes medium. The protein was isolated and purified according to the previously published protocols (*10*, *12*).

The NMR samples were prepared incubating the apoprotein in dithiothreitol (DTT) as reductant (20-fold molar excess to protein) in 100 mM phosphate buffer at pH 7.0. Then, the reductant concentration was equal to that of the protein. All manipulations were performed under inert atmosphere.

The copper-loaded samples were prepared as previously reported (*10*). The NMR samples had a concentration of about 2 mM with 1 equiv of DTT and 10% D_2O for the lock signal.

Structure Determination. The NMR experiments for signal assignment of apo BsCopZ were recorded on Bruker Avance 800, 700, and 500 spectrometers operating at 18.8, 16.4, and

[†] This work was supported by the European Community (Contract HPRI-CT-2001-00147), MIUR-COFIN, and by MIUR-FIRB (RBNE-01TTJW).

* Address correspondence to this author at the Centro di Risonanze Magnetiche, University of Florence. Tel: +39 055 4574272. Fax: +39 055 4574271. E-mail: ivanobertini@cerm.unifi.it.

[1] Abbreviations: *E. hirae*, *Enterococcus hirae*; *E. coli*, *Escherichia coli*; *B. subtilis*, *Bacillus subtilis*; Cu-ATPase, copper-transporting P-type adenosinetriphosphatase.

10.1021/bi0353326 CCC: $25.00
Published on Web 10/28/2003

Table 1: Acquisition Parameters of the NMR Experiments Performed on Apo BsCopZ

	acquired data points (nucleus)			spectral width (Hz)			field	
expt	t_3	t_2	t_1	F_3	F_2	F_1	(MHz)	ref
[^{1}H−^{1}H]-NOESY[a]	2048 (^{1}H)	1024 (^{1}H)		10416	10416		800	*28*
^{1}H−^{15}N-HSQC[a,b]	1024 (^{15}N)	256 (^{1}H)		9615	3333		800	*29*
^{15}N-edited [^{1}H−^{1}H]-NOESY[a]	1024 (^{1}H)	32 (^{15}N)	256 (^{1}H)	10416	3086	10416	800	*30*
^{15}N-edited [^{1}H−^{1}H]-NOESY[b]	1024 (^{1}H)	32 (^{15}N)	288 (^{1}H)	7507	2027	7507	500	*30*
^{15}N-edited [^{1}H−^{1}H]-TOCSY[a]	1024 (^{1}H)	64 (^{15}N)	256 (^{1}H)	9124	3125	9124	700	

[a] Experiments acquired at 300 K. [b] Experiments acquired at 298 K.

11.7 T, respectively. The latter spectrometer is equipped with a cryoprobe. All of the performed experiments are reported in Table 1.

The NMR data were processed with the XWinNMR software, and the spectral analysis was done with XEASY (*13*). For all spectra, shifted sine-bell functions were used to apodize the data. The data were zero-filled once in indirect dimensions before Fourier transformation.

The peaks used for structure calculations were integrated in the 2D NOESY and 3D ^{15}N-NOESY-HSQC experiments and converted into upper distance limits with the program CALIBA (*14*). Stereospecific assignments were obtained through the program GLOMSA (*14*) and through analysis of the HNHB experiment (*15*). $^3J_{HNH\alpha}$ coupling constants were obtained from the ratio between the intensity of the diagonal peak and the cross-peak in the HNHα map, and their values were correlated to the backbone torsion angles ϕ by means of the appropriate Karplus curve (*16*). ψ torsion angle constraints, for residue ($i-1$), were determined by measuring the intensity ratio of the $d_{\alpha N}(i-1,i)$ and $d_{N\alpha}(i,i)$ NOEs observed on the ^{15}N plane of residue i in the ^{15}N-NOESY-HSQC spectrum (*17*).

Structure calculation, refinement, and assessment were performed following the same approach used for the structure of the copper-bound form (*10*).

Structure Modeling and Energetic Analysis. Structures were modeled with the program MODELLER (*18*) using as reference the structure of apo CopZ from *Enterococcus hirae* (*19*) and the present structure of apo BsCopZ.

The program PROSA II (*20*) for protein structure energetic analysis was used to determine an adimensional energy term per residue, that is, a combination of pair interaction energies and surface energies.

RESULTS

Resonance Assignment, Structure Calculation, and Refinement of Apo BsCopZ. The ^{1}H−^{15}N-HSQC spectra of apo BsCopZ show a good dispersion of the signals, indicating that the protein is in a folded state. Some signals typical of unfolded species are also present with low intensity. As already established (*21*), the protein is in a dimeric form at millimolar concentrations. However, again as already described, the signal frequencies do not change upon dilution, indicating nonspecific aggregation (*21*).

The assignment of the protein signals was performed on the ^{15}N-labeled sample through analysis of ^{15}N-HSQC, 3D ^{15}N-TOCSY-HMQC, 3D ^{15}N-NOESY-HSQC, and 2D NOESY and TOCSY maps. About 92% of the total proton resonances were assigned, and 69 out of 72 peptidic NH cross-peaks were identified in the ^{15}N-HSQC spectra (the resonance assignment is reported as Supporting Information).

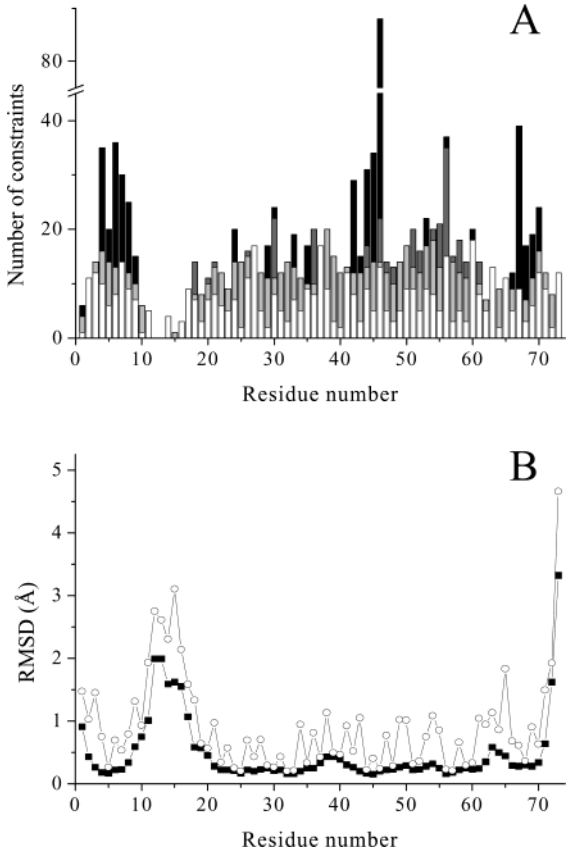

FIGURE 1: (A) Number of intraresidue (white), sequential (light gray), medium-range (gray), and long-range (black) NOEs per residue in apo BsCopZ. (B) Backbone (■) and heavy atom (○) rmsd values per residue for the family of 30 conformers with respect to the average minimized structure of apo BsCopZ.

In particular, NH cross-peaks are missing for residues 13−15 (loop 1), whereas cross-peaks of residues 11, 12, and 16−21 (loop 1 and helix α1) are significantly broadened. Furthermore, some residues belonging to loop 5 (62, 64−67) and helix α1 (*22*−*25*) display two conformations in a 70:30 ratio. The situation resembles that of yeast Atx1, another soluble copper chaperone, whose apo form shows few or no NOEs for the residues constituting loop 1 and the N-terminal part of helix α1 (*22*), and that of the fourth metal binding domain of Menkes copper-transporting ATPase (*23*).

A total of 1639 upper distance limits (of which 1431 were meaningful), 31 dihedral ϕ angle constraints, and 48 ψ angle constraints were measured and used in the structural calculations with the program DYANA (*24*). The average number of meaningful structural constraints per residue is 19.6. The number of experimental NOEs per residue, subdivided according to their class, is reported in Figure 1A. Sixteen stereospecific assignments were obtained.

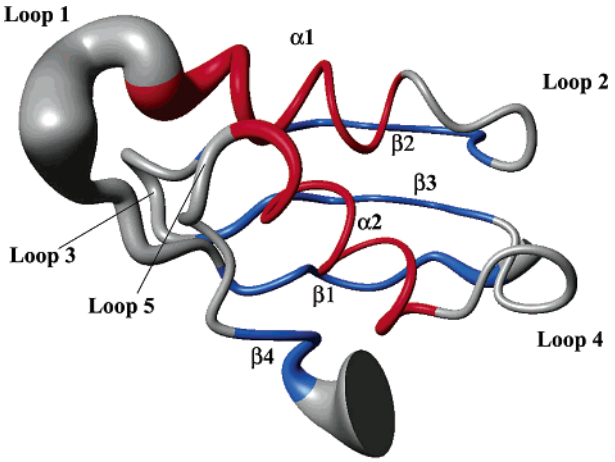

FIGURE 2: Solution structure of apo BsCopZ represented as a tube of radius proportional to the rmsd to the mean structure. Each conformer was aligned by best-fit superposition of C, Cα, and N atoms of residues 3−9 and 18−70. The secondary structure elements are shown in red (α-helices) and blue (β-strands).

A family of 30 conformers was obtained with an average target function of 0.86 ± 0.10 Å^2 (the best structure has a target function of 0.60 Å^2). After refinement through restrained energy minimization on each member, the final family has average rmsd values to the mean structure (for residues 4−70) of 0.61 ± 0.15 Å for the backbone and 1.13 ± 0.17 Å for the heavy atoms and a penalty function for the distance constraints, averaged over the family, of 0.33 ± 0.03 Å^2. The rmsd values calculated without residues 10−17 drop to 0.33 ± 0.08 Å for the backbone and 0.84 ± 0.07 Å for the heavy atoms. In Figure 1B the rmsd values per residue of the final REM family are reported. The NMR solution structure is shown in Figure 2. A statistical analysis of the conformer family and of the average structure is reported in Table 2.

Description of the Structure. The apo BsCopZ fold consists, like the copper-loaded form and other soluble copper chaperones (1, 4, 10), of a twisted four-stranded antiparallel β-sheet (2−7, 30−36, 41−46, 69−71) and two α-helices (16−25, 53−63) that are both located on the same side of the β-sheet (Figure 2).

The protein segments forming secondary structure elements are very well defined. On the contrary, the most disordered regions, besides the N- and C-terminal parts, are loop 1 (residues 8−15), the first two residues of helix α1 (residues 16 and 17), where one of the two copper ligands, Cys 16, is located, and, partially, loop 5. Loop 1 is external and contains Cys 13 and His 15 (both not identified) and Ser 12 and Gln 14 (partially identified). The lack of assignments produces a break in the sequential connectivities, and its external conformation determines a reduced number of NOEs for this region (Figure 1A). This behavior could reflect an increased flexibility in the copper binding region. Such flexibility is sizably reduced when the metal is present, as in this case resonances from all of the residues can be detected (*10*). Met 11, even if relatively disordered, has, out of the error, an external conformation pointing toward the solvent, as clearly defined by a few NOEs on the side chain ($H_{\gamma 1,2}$ Glu 9−$H_{\gamma 2}$ Met 11, $H_{\beta 2}$ Tyr 65−$H_{\beta 3}$ Met 11, $H_{\delta 1,2}$ Tyr 65−$H_{\beta 3}$ Met 11). Extensive hydrophobic interactions are connecting loops 1, 3, and 5. Cys 16, the first residue of helix α1, is completely buried (solvent accessibility 6%), particularly due to the interaction with the side chain of Leu 37 (solvent accessibility 9%) in loop 3. Leu 37 is a highly conserved residue which, in some sequences, is replaced by a Phe, again a hydrophobic residue. Also, Val 8 (loop 1, solvent accessibility 2%) contributes, through hydrophobic contacts with Leu 37, to the stabilization of the interactions between loop 1 and loop 3, which together form a hydrophobic patch, completely buried to the solvent, around the metal binding site. Also on loop 5, located at the same protein side as loops 1 and 3, a highly conserved residue, Tyr 65, is present; it assumes, however, an external position in the present structure.

Interaction Studies of Apo BsCopZ with Cu(I) BsCopZ. The exchange of copper between metal-loaded and apopro-

Table 2: Statistical Analysis of the REM Family and of the Mean Structure of Apo BsCopZ[a]

	REM (30 conformers)	⟨REM⟩ (average)
rms Violations per Experimental Distance (Å) and Angle (deg) Constraints[b]		
intraresidue (203)	0.0241 ± 0.0026	0.0225
sequential (392)	0.0095 ± 0.0018	0.0092
medium range[c] (346)	0.0102 ± 0.0012	0.0106
long range (490)	0.0141 ± 0.0015	0.0156
total (1431)	0.0143 ± 0.0008	0.0143
backbone torsion angle ϕ (31)	0.45 ± 0.45	0.0000
backbone torsion angle ψ (48)	0.71 ± 0.42	0.5857
Average Number of NOE Violations per Structure		
intraresidue	11.7 ± 1.3	12.0
sequential	5.5 ± 1.4	6.0
medium range[c]	7.6 ± 1.3	6.0
long range	15.4 ± 2.3	15.0
total	40.2 ± 3.1	39.0
backbone torsion angle ϕ	0.7 ± 0.7	0.0
backbone torsion angle ψ	1.2 ± 0.8	1.0
violations of NOE larger than 0.3 Å	0	0
violations of NOE between 0.1 and 0.3 Å	7.6 ± 2.1	9.0
average NOE penalty function (Å^2)	0.33 ± 0.03	0.32
average BB torsion angle penalty function (deg^2)	1.56 ± 0.54	0.29
Structural Analysis[d]		
% of residues in most favored regions	73.8	64.4 (69.0)[f]
% of residues in allowed regions	23.1	27.7 (27.6)[f]
% of residues in generously allowed regions	3.1	4.6 (3.4)[f]
% of residues in disallowed regions	0.0	3.1 (0.0)[f]
Experimental Restraint Analysis[e]		
% completeness of experimentally observed NOEs up to 4 Å cutoff distance	64.3	60.1
% completeness of experimentally observed NOEs up to 5 Å cutoff distance	45.8	42.1

[a] REM indicates the energy-minimized family of 30 structures; ⟨REM⟩ is the energy-minimized average structure obtained from the coordinates of the individual REM structures. [b] The number of experimental constraints for each class is reported in parentheses. [c] Medium-range distance constraints are those between residues *i*,*i*+2, *i*,*i*+3, *i*,*i*+4, and *i*,*i*+5. [d] As it results from the Ramachandran plot analysis on the secondary structure elements. [e] As it results from the AQUA analysis (*31*) over all of the residues of the protein (*32*). [f] Calculated with the exclusion of the disordered loop I (from 11 to 17).

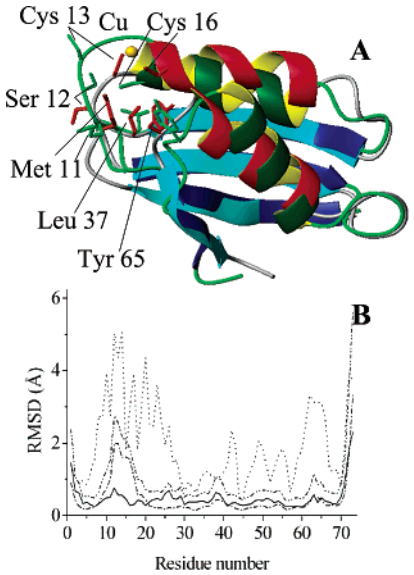

FIGURE 3: (A) Structures of the apo BsCopZ (green and blue) and of the Cu(I) BsCopZ (red, cyan, and gray) (superimposed fitting over residues 3−9 and 18−70). Relevant residues in loops 1, 3, and 5 are shown. (B) Backbone rmsd per residue (i) within the 30 conformer families of the apo BsCopZ (− · −) and (ii) Cu(I) BsCopZ (—) proteins and (iii) between the mean energy-minimized structures of the two families (···). The sum of the rmsd values per residue for the two families of structures is also shown (− ·· −).

teins has been investigated by means of $^{1}H-^{15}N$-HSQC experiments on the 50% mixture of the two species. The NH signals of the two species are not affected by the mixing. On the other hand, the signals of ^{15}N-labeled Cu(I) BsCopZ decrease in the presence of nonlabeled apo BsCopZ. Therefore, it can be concluded that copper exchange occurs but at a rate slower than 10^3 s^{-1}. On the contrary, the rate of copper transfer between the chaperones and the copper-receiving ATPases is larger than 10^3 s^{-1} (defined by the chemical shift differences between the two forms) (*1*, *12*, *25*), indicating that a synergistic action of the two proteins is needed.

DISCUSSION

Comparison with the Copper(I)-Loaded BsCopZ. The analysis of the ^{1}H, ^{15}N, and weight-averaged (*26*) chemical shift differences between apo and copper-loaded BsCopZ (*12*) highlights that the largest changes are located in loop 1, in the first turn of helix α1, in β2 (His 34), and in loop 5, with some smaller changes observed also in loop 3. The secondary structure elements of apo BsCopZ are the same in terms of type and extent as those in Cu(I) BsCopZ (*10*) (Figure 3A). Relevant are the exceptions of helix α1, which is shortened to residues 16−25 (it spans 14−24 in the copper-loaded form) with residues 16−17 experiencing high rmsd values, of strand β4, which is shortened to residues 69−71 (residues 67−71 in the copper-loaded form), and of strand β1 that is lengthened to residues 2−7 (residues 4−8 in the copper-loaded form). The global rmsd values between the apo and Cu(I) BsCopZ pair are 2.21 and 2.87 Å for the backbone and heavy atoms, respectively, when the entire protein is considered, while they decrease to 0.94 and 2.02 Å when only the four β-strands are considered. The two α-helices have intermediate rmsd values. When the rmsd between the two structures is compared to the sum of the rmsd values of the two families (which indicates if the

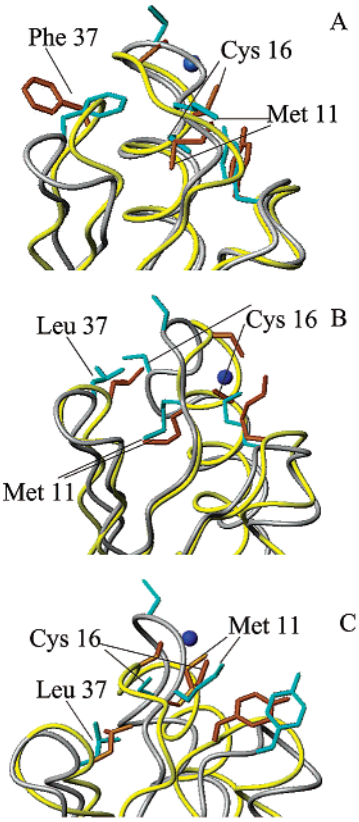

FIGURE 4: Close-up of the residues located in loops 1, 3, and 5 around the metal site for the apo (gray and cyan) and metal-loaded (yellow and orange) forms of MerP (A), yAtx1 (B), and BsCopZ (C). The blue sphere represents the copper ion.

structural differences are meaningful with respect to the structural uncertainties) (Figure 3B), it appears that the main differences in the global fold are located in the loops and α-helices. In the apo form, loop 1 moves toward the solvent and loop 5 increases its length, with the concomitant reduction in length of strand β4. A small translation of the last turn of helix α2 occurs, as well as a translation of helix α1 toward strand β2 and helix α2. The movement of helix α1 is supported by the change in several long-range NOEs of residues in this helix. As an example, NOESY cross-peaks were identified between $H_{\beta 2,3}$ of Ser 23 (α1) and $H_{\beta 2}$ of Gln 63 (β2) and between H_{α} of Val 24 and $CH_{3\gamma}$ of Val 30 in the apo form, which are not present in Cu(I) BsCopZ. These differences, and other sizable changes in NOE intensities, are in agreement with a slight movement of helix α2 when passing from Cu(I) to apo BsCopZ.

Met 11 has different conformations in the two protein forms: it is pointing toward the metal ion in the Cu(I)-loaded form, while it is completely solvent exposed in the apo form. This conformational change can be correlated with the rotation of the side chain of Tyr 65 [loop 5 (Figure 4)] which experiences a sizable change in solvent accessibility, from 26% to 52%, from the Cu(I)-loaded to the apo form. Hydrophobic contacts between Met 11 and Tyr 65 are present only in the copper-loaded form. On the contrary, the conformation of Cys 16 (helix α1), quite buried, determines an extended hydrophobic contact with Leu 37 only in the apo form. Cys 13, in loop 1, changes its conformation, becoming sizably solvent exposed in the apo form. The conformation of loop 3 is very similar in the two protein

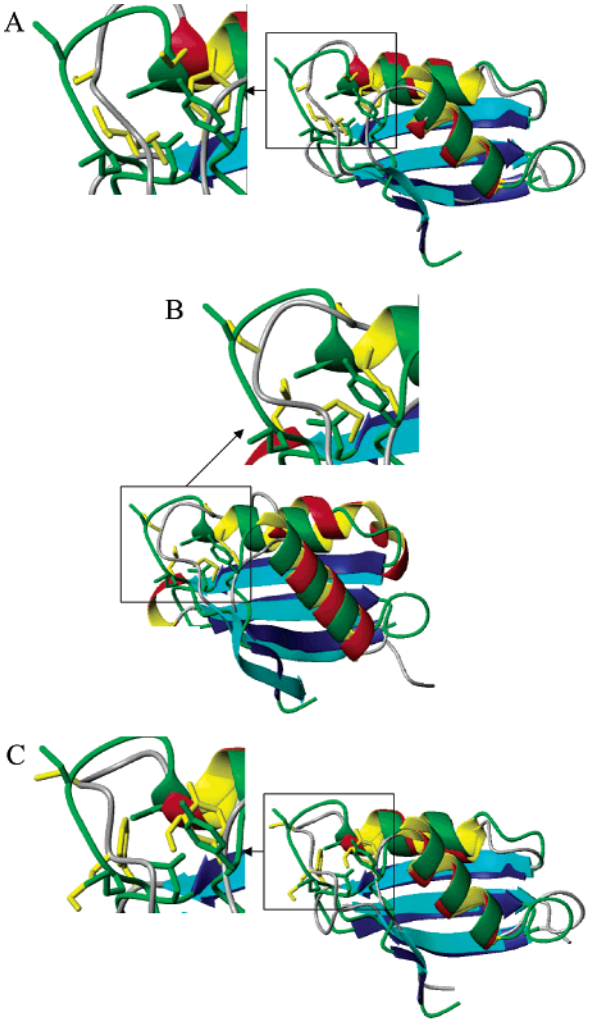

FIGURE 5: Structure of the apo BsCopZ (green and blue) compared with that of apo EhCopZ (A), apo yAtx1 (B), and apo MerP (C) (red, cyan, and gray). The two copper ligands are also reported.

forms, with Leu 37 making hydrophobic contacts with Val 8. Therefore, it results that, upon copper binding, residues located in loops 1 (or beginning of helix α1) and 5 change conformation depending on the presence or absence of copper, while loop 3 has the same conformation. In addition, the loops involved in hydrophobic interactions change from loop 1 with loop 3 to loop 1 with loop 5.

Comparison with EhCopZ, yAtx1, and MerP. BsCopZ shows a significant level of sequence identity with several metal chaperones. Among them, it has 39% identity with *E. hirae CopZ* (EhCopZ), a copper chaperone protein from a Gram-positive bacterium, 28% identity with yAtx1, a copper chaperone protein from yeast, and 35% identity with MerP, a mercury detoxification protein from Gram-negative bacteria (*5*). For all of these proteins the structures are available (*19*, *22*, *27*), and therefore, it is meaningful to compare the present structure with that of these proteins (residues are numbered according to the BsCopZ sequence).

In Figure 5A apo BsCopZ is compared to apo EhCopZ (*19*). The global fold and all of the secondary structure elements are maintained in the two proteins, the rmsd value for the backbone being 1.57 Å, excluding the residues in the copper binding loop. Loops 1, 3, and 5 show some differences between the two proteins, even if loop 1 assumes an analogous external conformation in both apo forms, as a consequence of the absence of the metal ion. Met 11, at variance with BsCopZ, assumes an internal conformation (17% solvent accessibility) making extensive hydrophobic contacts with Leu 37, which are now not present with Cys 16, despite its similar buried character.

Apo BsCopZ also shares the same fold with apo yAtx1 (*22*) (Figure 5B). Some differences are present in helix α1, shortened in apo yAtx1, and in loop 3, which in apo yAtx1 contains a 3_{10} helix. Similarly to EhCopZ, also in apo yAtx1, Met 11 is buried and makes extensive contacts with Leu 37. At variance with the other proteins, Cys 16 is significantly solvent exposed.

A further example of soluble metal-transporting proteins which exhibit the same fold as apo BsCopZ is represented by apo MerP (*27*) (Figure 5C); the structures of the two apoproteins present an rmsd value for the backbone (with the exclusion of loop 1) of 1.88 Å. Indeed, all of the elements of secondary structure are well conserved in length and reciprocal orientation. The loops have quite similar conformation with the exception of loop 3 which, in MerP, contains in position 37 an aromatic residue (Phe) whose orientation depends on the presence or absence of the metal ion (*27*). Still, Phe 37 makes extensive contacts with Cys 16, as occurs in apo BsCopZ. Significantly, Met 11 (BsCopZ numbering) assumes a solvent-exposed conformation similar to that of apo BsCopZ.

Changes in loops 1, 3, and 5 are detected, upon metal binding, also in yAtx1 and in MerP (for EhCopZ the structure of the copper-bound form is not available). In both apo yAtx1 and MerP, upon metal binding, loop 1 moves toward the solvent, as occurs also in BsCopZ. Cys 13, located in loop 1, has a sizable change in position and becomes completely solvent accessible (solvent accessibility from 21% and 15% to 37% and 42% in the two proteins, respectively). Cys 16 also undergoes some conformational change, but in both BsCopZ and MerP Cys 16 is completely buried, independently of the presence or absence of the metal, being located in the hydrophobic patch formed by loops 1, 3, and 5. On the contrary, in apo yAtx1 it becomes sizably solvent exposed at variance with the metal-loaded form. In yAtx1 Cys 16 is too far, however, from Leu 37 to interact with it, and then the latter residue is stabilized by interactions with Met 11, which assumes a more internal position, getting closer to the metal ion in both apo and copper-loaded forms. When the Leu in position 37 is replaced by other hydrophobic residues, such as Phe 37 in MerP, some variability in the conformation of Met 11 is observed. Still, hydrophobic contacts between residues of loop 1 (or beginiing of helix α1) and loop 3 are present in the apo form (Figure 6). In loop 5 at position 65 an aromatic residue (Phe/Tyr) is always present in bacterial proteins. van der Waals interactions between loops 1 and 5 are present in the metalated forms and not in the apo forms, with Met 11 making hydrophobic contacts with Tyr/Phe 65 (Figure 6). In eukaryotic proteins, position 65 is invariably occupied by a Lys which can still make contacts with residues in loop 1.

To assess these tight interactions between these loops and the contribution of residue conformation on the overall structural stability, we have modeled the structures of the proteins, interchanging the conformation of Met 11 with that of the other structures. When a PROSA-type analysis is performed on apo BsCopZ, where an internal orientation is

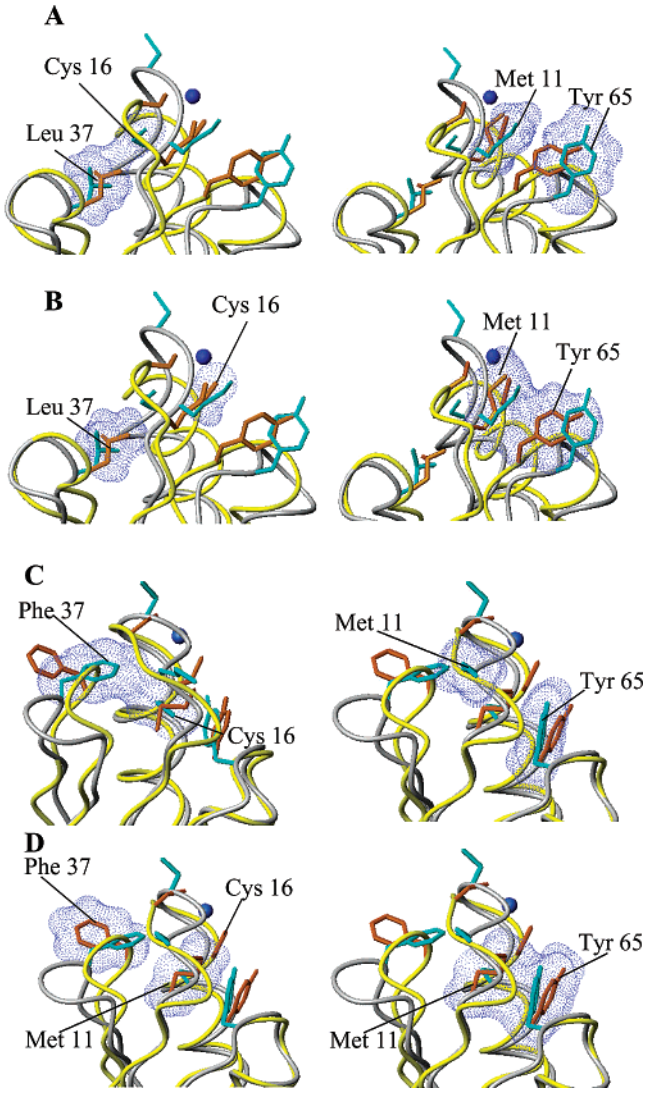

FIGURE 6: van der Waals interactions involving loops 1, 3, and 5 for (A) apo BsCopZ, (B) Cu(I) BsCopZ, (C) apo MerP, and (D) Hg(II) MerP. The color code is as in Figure 4.

imposed to Met 11, it appears that lower energies for residues in loop 1 (Met 11 and Cys 13) and in loop 5 (Tyr 65) are obtained but increased energies are induced on residues in loop 3 (Leu 37). Analogous behaviors are shown by all of the modeled structures independently of the original orientation of the Met 11.

Summarizing, it results from the present analysis that meaningful hydrophobic interactions are present around the metal site in all of the analyzed proteins and that they are modulated by the metal binding.

CONCLUSIONS

The comparison of the present structure with those of related proteins shows that all of these metallochaperones experience the same fold and that in the apo forms loop 1 moves toward the solvent with respect to the conformation of the copper-loaded protein. Meaningful differences, even if in most cases minor, essentially involve only the metal binding loop, the relative position/orientation of some helices which point to the metal binding site, and the loops located close to the metal coordination site.

The orientation of helix α1, as well as the conformation of loop 1 and possibly of loops 5 and 3, might have a role in the efficiency of the metal-transfer process and in the specificity of molecular recognition with the partner. The residues forming loop 1 and the N-terminal part of helix α1 (copper site) in most of the cases (BsCopZ, yAtx1, and MerP) take an external orientation in the apo form at variance with the metal-loaded proteins and experience sizable conformation exchange processes (*21*, *25*, *27*). The hydrophobic protection due to the Met11/Tyr65 moiety, which, in the copper-loaded proteins, sizably reduces the copper site solvent accessibility (*21*), is not present in the apo forms, as a consequence of the new orientation of loop 1 toward the solvent. It has been suggested that this partial protection in the copper-loaded forms might be relevant for determining the correct conformation at the copper site for the incoming copper-receiving protein (*10*). This new conformation could favor the incoming or outgoing of the copper ion in the copper site of the protein.

A tight connection, all originating from hydrophobic interactions, is holding loops 1, 3, and 5 to form an hydrophobic patch around the metal site (Figure 6). Changes in sequence and in amino acid conformation can induce local changes in the specific contacts still maintaining the global loop interactions. From a comparative structural analysis, a general pattern for the interactions among the odd loops of the proteins appears. In the apo forms of chaperone proteins, like BsCopZ, EhCopZ, and MerP, extended van der Waals contacts between residue 37 (Phe/Leu, loop 3) and residues 11 or 16 (loop 1 region) are present while van der Waals contacts between Met 11 and residue 65 (Tyr/Phe, loop 5) are significantly reduced or null. In particular, when Met 11 is external, the loop 1/loop 3 interaction is held by the AA 37/Cys 16 contact, while the latter residue is replaced by Met 11 when the latter assumes a buried conformation.The opposite happens in the metal-loaded forms of these proteins [Hg(II) MerP and Cu(I) BsCopZ], where hydrophobic contacts are connecting loop 1 (Met 11 or Cys 16) with loop 5 (Tyr/Phe) while those between loops 1 and 3 are not present.

This behavior is probably related to the tightly controlled interactions which link these three loops and which create an hydrophobic patch around the metal ion. This patch is a key aspect for the interaction with the partner. While long-range molecular recognition is modulated by electrostatic guidance, as witnessed by the complementarity of electrostatic potential surfaces (*5*, *12*, *25*), local interactions between the two metal binding sites and optimization of their conformations are more dependent on hydrophobic interactions. The tight connection between these loops is further supported by the results of interaction studies between BsCopZ and its partner BsCopA (*12*). When the two proteins interact, in addition to changes in residues of loops 1 and 5 and helix α1 and α2, significant changes in the chemical shifts are also observed for residues of loop 3 (*12*).

In conclusion, this study discusses a complex and intriguing pattern of interactions which are essential for modulating the optimal interactions with the partner and for the metal transfer process. The change in hydrophobic interactions between the two protein forms (apo versus metalated) could represent a switch for the protein recognition in the correct metalation state and could contribute to the thermodynamics of the metal transfer process.

ACKNOWLEDGMENT

Thanks are expressed to Fiorenza Cramaro for comments.

SUPPORTING INFORMATION AVAILABLE

^{15}N and ^{1}H resonance assignments for the apo BsCopZ in 100 mM phosphate buffer and 1 equiv of DTT, pH 7.0, at 300 K and experimental NOE intensity constraints with a list of stereospecific assignments, used for the structure calculations. This material is available free of charge via the Internet at http://pubs.acs.org.

REFERENCES

1. Finney, L. A., and O'Halloran, T. V. (2003) Transition Metal Speciation in the Cell: Insights from the Chemistry of Metal Ion Receptors, *Science 300*, 931−936.
2. Harrison, M. D., Jones, C. E., Solioz, M., and Dameron, C. T. (2000) Intracellular copper routing: the role of copper chaperones, *Trends Biochem. Sci. 25*, 29−32.
3. Puig, S., and Thiele, D. J. (2002) Molecular mechanisms of copper uptake and distribution, *Curr. Opin. Chem. Biol. 6*, 171−180.
4. Banci, L., and Rosato, A. (2003) Structural genomics of proteins involved in copper homeostasis, *Acc. Chem. Res. 36*, 215−221.
5. Arnesano, F., Banci, L., Bertini, I., Ciofi-Baffoni, S., Molteni, E., Huffman, D. L., and O'Halloran, T. V. (2002) Metallochaperones and metal transporting ATPases: a comparative analysis of sequences and structures, *Genome Res. 12*, 255−271.
6. Opella, S. J., DeSilva, T., and Veglia, G. (2002) Structural biology of metal-binding sequences, *Curr. Opin. Struct. Biol. 6*, 217−223.
7. Cavet, J. S., Borrelly, G. P., and Robinson, N. J. (2003) Zn, Cu and Co in cyanobacteria: selective control of metal availability, *FEMS Microbiol. Rev. 27*, 165−181.
8. Banci, L., Bertini, I., Ciofi-Baffoni, S., Finney, L. A., Outten, C. E., and O'Halloran, T. V. (2002) A new zinc-protein coordination site in an intracellular metal trafficking: solution structure of the apo and Zn(II) forms of ZntA(46−118), *J. Mol. Biol. 323*, 883−897.
9. Huffman, D. L., and O'Halloran, T. V. (2001) Function, structure, and mechanism of intracellular copper trafficking proteins, *Annu. Rev. Biochem. 70*, 677−701.
10. Banci, L., Bertini, I., Del Conte, R., Markey, J., and Ruiz-Dueñas, F. J. (2001) Copper trafficking: the solution structure of *Bacillus subtilis* CopZ, *Biochemistry 40*, 15660−15668.
11. Rosenzweig, A. C., and O'Halloran, T. V. (2000) Structure and Chemistry of the Copper Chaperone Proteins, *Curr. Opin. Chem. Biol. 4*, 140−147.
12. Banci, L., Bertini, I., Ciofi-Baffoni, S., Del Conte, R., and Gonnelli, L. (2003) Understanding copper trafficking in bacteria: interaction between the copper transport protein CopZ and the N-terminal domain of the copper ATPase CopA from *Bacillus subtilis*, *Biochemistry 42*, 1939−1949.
13. Eccles, C., Güntert, P., Billeter, M., and Wüthrich, K. (1991) Efficient analysis of protein 2D NMR spectra using the software package EASY, *J. Biomol. NMR 1*, 111−130.
14. Güntert, P., Braun, W., and Wüthrich, K. (1991) Efficient computation of three-dimensional protein structures in solution from Nuclear Magnetic Resonance data using the program DIANA and the supporting programs CALIBA, HABAS and GLOMSA, *J. Mol. Biol. 217*, 517−530.
15. Archer, S. J., Ikura, M., Torchia, D. A., and Bax, A. (1991) An alternative 3D NMR technique for correlation backbone ^{15}N with side chain Hβ resonances in larger proteins, *J. Magn. Reson. 95*, 636−641.
16. Vuister, G. W., and Bax, A. (1993) Quantitative J Correlation: A New Approach for Measuring Homonuclear Three-Bond J(H^NH^α) Coupling Constants in ^{15}N Enriched Proteins, *J. Am. Chem. Soc. 115*, 7772−7777.
17. Gagne', R. R., Tsuda, S., Li, M. X., Chandra, M., Smillie, L. B., and Sykes, B. D. (1994) Quantification of the calcium-induced secondary structural changes in the regulatory domain of troponin-C, *Protein Sci. 3*, 1961−1974.
18. Sali, A., and Blundell, T. L. (1993) Comparative protein modelling by satisfaction of spatial restraints, *J. Mol. Biol. 234*, 779−815.
19. Wimmer, R., Herrmann, T., Solioz, M., and Wüthrich, K. (1999) NMR structure and metal interactions of the CopZ copper chaperone, *J. Biol. Chem. 274*, 22597−22603.
20. Sippl, M. J. (1993) Recognition of Errors in the Three-Dimensional Structures, *Proteins: Struct., Funct., Genet. 17*, 355−362.
21. Banci, L., Bertini, I., Del Conte, R., Mangani, S., and Meyer-Klaucke, W. (2003) X-ray absorption spectroscopy study of CopZ, a copper chaperone in *Bacillus subtilis*. The coordination properties of the copper ion, *Biochemistry 8*, 2467−2474.
22. Arnesano, F., Banci, L., Bertini, I., Huffman, D. L., and O'Halloran, T. V. (2001) Solution Structure of the Cu(I) and Apo forms of the Yeast Metallochaperone, Atx1, *Biochemistry 40*, 1528−1539.
23. Gitschier, J., Moffat, B., Reilly, D., Wood, W. I., and Fairbrother, W. J. (1998) Solution structure of the fourth metal-binding domain from the Menkes copper-transporting ATPase, *Nat. Struct. Biol. 5*, 47−54.
24. Güntert, P., Mumenthaler, C., and Wüthrich, K. (1997) Torsion Angle Dynamics for NMR Structure Calculation with the new program DYANA, *J. Mol. Biol. 273*, 283−298.
25. Arnesano, F., Banci, L., Bertini, I., Cantini, F., Ciofi-Baffoni, S., Huffman, D. L., and O'Halloran, T. V. (2001) Characterization of the binding interface between the copper chaperone Atx1 and the first cytosolic domain of Ccc2 ATPase, *J. Biol. Chem. 276*, 41365−41376.
26. Garrett, D. S., Seok, Y. J., Liao, D. I., Peterkofsky, A., Gronenborn, A. M., and Clore, G. M. (1997) N-terminal domain of enzyme I of the *Escherichia coli* phosphoenolpyruvate: sugar phosphotransferase system by multidimensional NMR, *Biochemistry 36*, 2517−2530.
27. Steele, R. A., and Opella, S. J. (1997) Structures of the reduced and mercury-bound forms of MerP, the periplasmic protein from the bacterial mercury detoxification system, *Biochemistry 36*, 6885−6895.
28. Macura, S., Wüthrich, K., and Ernst, R. R. (1982) The relevance of *J* cross-peaks in two-dimensional NOE experiments of macromolecules, *J. Magn. Reson. 47*, 351−357.
29. Sklenar, V., Piotto, M., Leppik, R., and Saudek, V. (1993) Gradient-tailored water suppression for ^{1}H-^{15}N HSQC experiments optimized to retain full sensitivity, *J. Magn. Reson., Ser. A 102*, 241−245.
30. Wider, G., Neri, D., Otting, G., and Wüthrich, K. (1989) A Heteronuclear Three-Dimensional NMR Experiment for Measurements of Small Heteronuclear Coupling Constants in Biological Macromolecules, *J. Magn. Reson. 85*, 426−431.
31. Laskowski, R. A., Rullmann, J. A. C., MacArthur, M. W., Kaptein, R., and Thornton, J. M. (1996) AQUA and PROCHECK-NMR: Programs for checking the quality of protein structures solved by NMR, *J. Biomol. NMR 8*, 477−486.
32. Laskowski, R. A., MacArthur, M. W., and Thornton, J. M. (1998) Validation of protein models derived from experiment, *Curr. Opin. Struct. Biol. 8*, 631−639.

BI0353326